Available online at www.sciencedirect.com

ScienceDirect

journal homepage: www.elsevier.com/locate/he

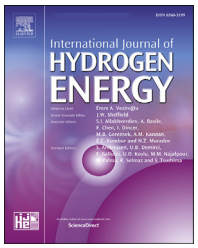

Semiconductor Fe-doped $SrTiO_{3-\delta}$ perovskite electrolyte for low-temperature solid oxide fuel cell (LT-SOFC) operating below 520 °C

M.A.K. Yousaf Shah [a,1], Sajid Rauf [b,1], Naveed Mushtaq [b], Zuhra Tayyab [b], Nasir Ali [c], Muhammad Yousaf [b], Yueming Xing [a], Muhammad Akbar [b], Peter D. Lund [d,e], Chang Ping Yang [b,***], Bin Zhu [a,b,d,e,*], Muhammad Imran Asghar [b,d,**]

[a] Engineering Research Center of Nano-Geo Materials of Ministry of Education, Department of Materials Science and Chemistry, China University of Geosciences, 388 Lumo Road, Wuhan, 430074, China

[b] Hubei Collaborative Innovation Center for Advanced Organic Chemical Materials, Faculty of Physics and Electronic Science, Hubei University, Wuhan, Hubei, 430062, China

[c] Zhejiang Province Key Laboratory of Quantum Technology and Devices and Department of Physics and State Key Laboratory of Silicon Materials, Zhejiang University, Hangzhou, 310027, China

[d] New Energy Technologies Group, Department of Applied Physics, Aalto University School of Science, P. O. Box 15100, FI-00076 Aalto, Espoo, Finland

[e] School of Energy and Environment, Southeast University, No.2 Si Pai Lou, Nanjing 210096, China

HIGHLIGHTS

- SrFe0.2, 0.3TiO3-δ (SFT) single-phase semiconductor utilized as an electrolyte in SOFC.
- SrFexTi1-xO3-ä(x = 0.3) has revealed high ionic conductivity of 0.17 S/cm at 520 °C.
- Fuel-cell based SrFexTi1-xO3-δ(x = 0.3) electrolyte has demonstrated impressive performance of 540 mW/cm2 at 520 °C.

ARTICLE INFO

Article history:
Received 20 January 2020
Received in revised form
13 March 2020
Accepted 18 March 2020
Available online 18 April 2020

ABSTRACT

High-temperature operation of solid oxide fuel cells causes several degradation and material issues. Lowering the operating temperature results in reduced fuel cell performance primarily due to the limited ionic conductivity of the electrolyte. Here we introduce the Fe-doped $SrTiO_{3-\delta}$ (SFT) pure perovskite material as an electrolyte, which shows good ionic conduction even at lower temperatures, but has low electronic conduction avoiding short-circuiting. Fuel cell fabricated using this electrolyte exhibits a maximum power density of 540 mW/cm^2 at 520 °C with Ni-NCAL electrodes. It was found that the Fe-doping into the $SrTiO_{3-\delta}$ facilitates the creation of oxygen vacancies enhancing ionic conductivity and

* *Corresponding author*. Engineering Research Center of Nano-Geo Materials of Ministry of Education, Department of Materials Science and Chemistry, China University of Geosciences, 388 Lumo Road, Wuhan, 430074, China.
** *Corresponding author*. Hubei Collaborative Innovation Center for Advanced Organic Chemical Materials, Faculty of Physics and Electronic Science, Hubei University, Wuhan, Hubei, 430062, China.
*** *Corresponding author*.
E-mail addresses: cpyang@hubu.edu.cn (C.P. Yang), binzhu@kth.se, binzhu@cug.com (B. Zhu), imran.asghar@aalto.fi (M.I. Asghar).
[1] Authors have contributed equally.

https://doi.org/10.1016/j.ijhydene.2020.03.147

Keywords:
Low-temperature solid oxide fuel cell (LT-SOFC)
Semiconductor electrolyte SFT
Band alignment
Impressive fuel cell performance & high ionic conduction

transport of oxygen ions. Such high performance can be attributed to band-bending at the interface of electrolyte/electrode, which suppresses electron flow, but enhances ionic flow.

Introduction

The properties of semiconductors enable their application in various fields, including optoelectronics and electrochemical devices [1]. On the other hand, in the electrochemical devices, particularly, solid oxide fuel cell (SOFCs) is still facing the critical challenge in commercialization due to its high operating temperature and stability [2–4]. It is widely accepted that solid electrolyte plays a central role in realizing the fuel cell function in SOFC [5]. Yttrium stabilized zirconia (YSZ) is a high-temperature dependent electrolyte (650 °C–1000 °C operating temperature), and a thickness of 10 μm has been often used as an electrolyte due to its higher ionic ~ 0.1 S/cm conduction. The higher operational temperature >800 °C has led the device to slow start-up and shut-down, expensive materials, and higher degradation rate in the performance of fuel cells. The fuel cell society has taken this issue to overcome these severe problems, and worldwide attempts are geared up to lower the temperature <600 °C for commercialization of LT-SOFC [6]. In this regard, the key is to develop sufficient ionic conducting electrolyte materials working at low temperatures (300–500 °C). Therefore, at least high ionic conductivity of >0.1 S/cm at low temperature (300–500 °C) is the main prerequisite to optimize the fuel cell technology from different prospective such as performance, cost and stability.

To avail this opportunity worlds has led their path to the semiconductor materials which are used as the electrodes, mostly the cathodes, like perovskite oxides, MNO_3 (M = Sr, Ba, Ca, La, Sm, etc.; N=Mn, Fe, Co, Ni etc.) and $La_{0·3}Sr_{0·7}Fe_{0·7}Ti_{0·3}O_3$ (LSFT) based materials in SOFCs. Besides, there are rare materials reported replacing the electrolyte by introducing the ionic conductivities in these SOFC perovskite cathode materials [7]. In addition, the semiconductors and their composites have been recently discovered with high ionic conductivity leading to LT-SOFCs [8–12]. By using the higher ionic property of electrolyte to make advanced fuel cell applications as compared to other materials but at low temperature. Recently, semiconductor $CeO_{2-\delta}$ has been used as an electrolyte to construct the fuel cell device in the configuration of NCAL/$CeO_{2-\delta}$/NCAL and NCAL/$CeO_{2-\delta}$/CeO_2/NCAL. Xing et al. have designed the fuel cell NCAL/$CeO_{2-\delta}$/NCAL based on core/shell idea have demonstrated a marvelous power output 697 mW/cm^{-2} and high proton conductivity 0.16 S/cm at low temperature 520 °C. Similarly, Wang et al. have used the core/shell idea in designing the fuel cell (NCAL/$CeO_{2-\delta}$/CeO_2/NCAL) and delivered the maximum power output 660 mW/cm^{-2} and impressive ionic conductivity 0.1 S/cm at 550 °C [10,13]. Zhou et al. have reported $SmNiO_3$ (SNO) as an electrolyte to construct the fuel cell device in the configuration of Pt/SNO/Pt. These proton conducting fuel cells have produced 225 mW/$cm^{2,}$ which is the best performance achieved at 500 °C with a high open-circuit voltage (OCV) of 1.03 [14].

Before semiconductor and their heterostructure, Zhu et al. reported the single layer electrolyte separator free fuel cell (EFFC) containing an ionic and semiconducting heterostructure layer that involves the same electrochemical reaction as in conventional fuel cell [12,15,16]. This invention was highlighted as "Three in one" because the one-layer device can realize the function of all components of fuel cells [15]. Also, Fan et al. have suggested that nano-thin films and nanomaterial are useful to produce better efficiency of fuel cells [17]. Moreover, the semiconductor and its heterostructure materials have been reported as an electrolyte. These electrolytes contain mix conducting (electronic & ionic) properties having unique features like energy band and band bending, consequently generate the built-in field and promote electron/hole conduction of semiconductors [18]. All of these properties of semiconductor and its heterostructure have been used in fuel cell technology leading to construct an appropriate low-temperature electrolyte; consequently, a large number of semiconductor-based electrolytes have been reported [9,19–22]. Such as, Chen et al. have reported semiconductor La–$SrTiO_3$ electrolyte, which exhibited super-ionic conduction (0.221 S/cm at 550 °C) induced by surface layer in a core-shell structure while operated in fuel cells [19]. Also, there is some newly reported electrolyte that has exhibited the best performance as well as effective ionic conductivity [23,24].

Despite the above-reported literature, there is some other promising semiconductor perovskite that possessed substantial ionic conduction but still has not been applied as an electrolyte. Such as $SrFeO_{3-\delta}$ redox stable perovskite can cause to obtain the higher O-vacancies by incorporation of Ti on B-side of the Perovskite, which overall leads to increased ionic conductivity [25]. These outcomes manifest that semiconductor can hold a great potential to be applied as an electrolyte although have low power output. There are many data reported for SFT perovskite, but the reported ionic conductivity and performance are smaller, and working condition temperature is higher. In addition, the SFT has been reported as a cathode, but here we have reported it as a single-phase electrolyte membrane [25–27].

Inspiring from the above studies, we have successfully prepared the $SrFe_xTi_{1-x}O_{3-\delta}$(x = 0.2, 0.3) (SFT) semiconductor

electrolyte via the co-precipitation method. As we know, the transportation of an electron in a semiconductor material is related to the energy band structure; as a result, we design a material bandgap to suppress the electronic transport in electrolyte and prevent the device from the short-circuiting issue. Besides, it was observed that the doping effect of Fe could cause to produce O-vacancies, which overall enhances the ionic conduction of the device. As a result, our device $SrFe_xTi_{1-x}O_{3-\delta}$(x = 0.3) has demonstrated excellent performance 540 mW/cm^2 as well as higher ionic conduction 0.17 S/cm at low-temperature 520 °C. While $SrFe_xTi_{1-x}O_{3-\delta}$(x = 0.2) has revealed the performance of 322 mW/cm^2 along with good ionic conduction 0.12 S/cm at low temperature 520 °C which is quite lower than the $SrFe_xTi_{1-x}O_{3-\delta}$(x = 0.3). It is also thought that this study will help to extend the single-phase semiconductor to be used in fuel cell technology to achieve even better performance.

Materials and method

$Sr1Fe_xTi_{1-x}O_{3-\delta}$ (x = 0.2, 0.3) perovskite oxide was prepared via co-precipitation method using Na_2CO_3 as a precipitant agent. In detail, 1 mol of pure $Sr(NO_3)_2$ (Sigma 99.9%), 0.2,0.3 mol of $Fe(NO_3)_2$ (Sigma 99.9%), and 0.8,07 mol of prepared $Ti(NO_3)_2$ (dissolving an appropriate ratio of TiO_2 (Sigma 99.9%) in (HNO_3 – 66% purity) and engaged as a cation precursor. In detail the chemical formula of our material is $Sr_1Ti_{1-x}Fe_xO_{3-\delta}$ (x = 0.2 and 0.3). Following the chemical formula, 1 mol of $Sr(NO_3)_2$, while 0.8, and 0.7 mol of TiO_2 were used to obtain the required perovskite structure, respectively. Firstly, TiO_2 was dissolved in HNO_3 to obtain $Ti(NO_3)_2$ and was added into another solution of $Sr(NO_3)_2$ and $Fe(NO_3)_2$ prepared in deionized water. The calculated amount of above-stated cations precursor was liquefied into the as-prepared solution, and then a certain amount of precipitating agent Na_2CO_3 dissolved in DI water to obtain a homogenous solution. The precipitating agent was added into the as-prepared solution; as a result, white precipitates were obtained. The solution was certified to stir for 6 h; afterward, the precipitates were filtered to obtain the SFT materials. The precipitate after the infiltration was washed much carefully with distilled water to remove the Na_2CO_3 from the surface of $Sr_1Ti_{1-x}Fe_xO_{3-\delta}$ (x = 0.2 and 0.3) (SFT).

Furthermore, the obtained precipitates were dried at 120° later dried materials were grounded to get the homogenous powder followed by sintering at 900 °C for 6 h. Then ground the powder in pestle mortal very well to obtain a homogenous powder of various ratios of Fe doped SF_xT_{1-x} (x = 0.2, 0.3) powders. The commercially purchased $LiNi_{0.8}Co_{0.15}Al_{0.05}O_2$ (NCAL) from Tianjin Bamo Company (TBC) was used as electrodes on both sides of the electrolyte layer $SrFe_{0.3}Ti_{0.7}O_{3-\delta}$ (SFT). The thickness, diameter, and area of pellet were 1 mm, 13 mm and 0.64 cm^2 respectively prepared under the pressure of 200–300 MPa and in the same manner other cell was fabricated. Before the cell performance measurements, these pellets were sintered at 650 °C for 1 h. Usually, our fuel cell operated at low-temperature (400–550 °C). However, the reason for sintering at such high-temperature possibly causes the oxidation of Ni-foam that will depreciate the Ni-NCAL electrode structure and current collection ability of Ni-foam. At last, the silver paste was applied on both sides of the pellet for fuel cell performance.

The diffraction pattern of prepared materials was characterized via an advanced x-ray diffractometer named Bruker D-8, Germany with Cu K alpha as a source of radiation, and detection of phase is performed at 40 kV and 40 mA. The morphology of the resulted materials was studied through Field Emission-scanning electron microscopy using the FE-SEM JEOL JSM7100 F machine made of Japan attached an Oxford energy dispersive spectrometer (EDS). To study morphology in detail, Transmission Electron Microscopy (TEM) was performed using (FEI Tecnai G2 F20 JEOL) machine, which operates at a voltage of 200 kV. An electrochemical workstation named as (Gamry reference 3000) was utilized to characterize the electrochemical impedance spectroscopy (EIS) works with 10 mV of ac signal in a frequency range of 0.1 Hz to 10^5 MHz of frequency under the H_2/air environments. The total electrical conductivity of the cell was obtained from the electrochemical impedance spectroscopy (EIS) data.

In contrast, the ionic conductivity was obtained from the ohmic resistance of the current-voltage (I–V) curve of the fuel cell. The Ultra-photoelectron spectroscopy with He–I (21.2 eV) discharge lamp and 100 meV of total energy resolution were implemented to attain the valence band maxima. Also, UV–visible absorption spectra with UV-3600 spectrometer were tested to determine the optical properties such as bandgap.

Result and discussion

X-ray diffraction (XRD)

Fig. 1 presents the X-ray diffraction pattern of $SrFeTiO_{3-\delta}$ (SFT) with different Fe doping ratio obtained through x-ray diffractogram named as Bruker D-8 containing Cu K-α lemda = 1.54 as a source of radiations. All diffraction peaks can well be indexed as a simple cubic perovskite structure. Fe doping with different ratio neither shown secondary phase nor any impurity, which demonstrate that Fe is well doped

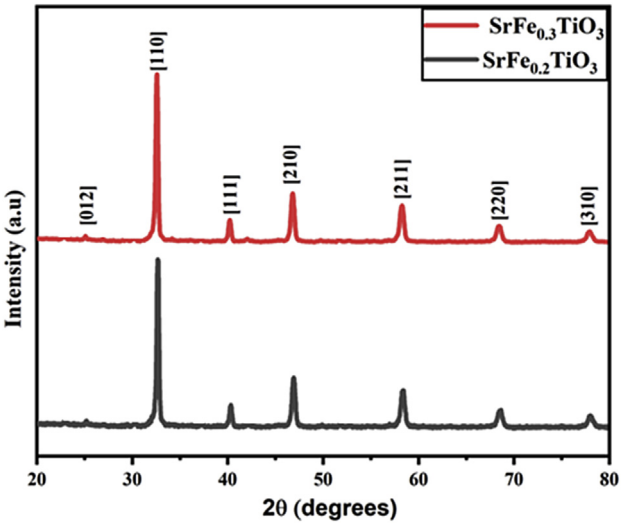

Fig. 1 – X-ray diffraction pattern of the prepared $SrFe_{0.2}TiO_{3-\delta}$ and $SrFe_{0.3}TiO_{3-\delta}$ electrolyte material.

displayed in XRD pattern. The characteristics peaks with [hkl] values of [012], [110], [111], [210], [211], [220], and [310] indexed to SFT were corresponded to pure perovskite structure with JPCD # 330677, and also it is well accordance to previously reported literature [25,26,28]. The peaks shifted towards the lower angle upon the increasing concentration of the dopant Fe, signifying that Fe is well doped and also lattice parameter changes via expanding the unit cell structure [25].

The calculated lattice parameter using the Sherrer formula $D = K\lambda/L(\cos\theta)$ is 3.879 Å and 3.89605 Å, indicating that the lattice parameter increased via increasing the dopant concentration. This might happened due to the difference in the ionic radius of Fe and Ti following the Vegards Law; the diffraction pattern is well-matched with the reported literature [29,30].

Furthermore, scanning electron microscopy (SEM) has been employed to investigate the morphology of $SrFe_xTi_{1-x}O_{3-\delta}$($x = 0.2, 0.3$). Fig. 2(a–b) illustrates the surface morphology of SFT extracted at the same size 1um, which confirms that all particles are uniformly distributed and well merged, which might contribute to the better electrochemical performance of fuel cell [22]. Also, TEM images revealed the presence of nano-sized particles; it can be differentiated that $SrFe_xTi_{1-x}O_{3-\delta}$($x = 0.3$) (SFT 30%) is denser (higher doping) than the $SrFe_xTi_{1-x}O_{3-\delta}$($x = 0.2$) (SFT 20%) as viewed in Fig. 2(c–d) respectively. The interconnection between particles may provide an easy path for the transportation of ions. The EDX supported by FE-SEM inculcates us that the Fe is well doped and uniformly distributed according to the doping ratio in SFT electrolyte semiconductor, as presented in Fig. 2(e–h).

Fuel cell performance

Fig. 3(a and b) shows the typical current-voltage (I–V) and current-power (I–P) characteristics of $SrFe_{0.2}TiO_{3-\delta}$ (SFT 20%) and $SrFe_{0.3}TiO_{3-\delta}$ (SFT 30%) electrolytes with symmetrical electrodes NCAL operated under H_2/air environments at 420–520 °C. As gases (H_2/air) environments were supplied; as a result, the maximum of 1V OCV was achieved within 200 s and then attained stabilized at 1.1 V almost after 450 s. Such higher OCV indicates neither gas leakage nor short-circuiting problem occurs as reported in published reports [31,32].

A maximum power density of 540 mW/cm^2 for $SrFe_xTi_{1-x}O_{3-\delta}$($x = 0.3$) has demonstrated while 322 mW/cm^2 power density obtained for $SrFe_xTi_{1-x}O_{3-\delta}$($x = 0.2$) for 30% and 20% doping respectively, excluding the possibilities of the short-circuiting. Such stabilized 540 mW/cm^2 performance is either comparable or lower than the reported reports [33,34]. The main reason for lower performance is the thin film and utilized micro-technology used in the fuel cell, but our power output is still better with such a formal method of cell preparation [35,36]. The $SrFe_xTi_{1-x}O_{3-\delta}$($x = 0.2$) electrolyte has demonstrated inferior performance than the $SrFe_xTi_{1-x}O_{3-\delta}$($x = 0.3$) electrolyte, which mainly happened due to the doping of Fe into STO because the acceptable higher doping ratio increase the creation of oxygen vacancies consequently increases the higher ionic conduction. While as we enhance the doping of Fe to more than 30%, it can cause to bring more defects, which overall cause to bind the fuel cell performance and conduction of charges. The results of more than 30% doping are not included. Briefly, the higher OCV and better performance confirm the usage of SFT semiconductor as an electrolyte in LT-SOFC signifies SFT maintaining the potential of both properties either as an electrolyte and cathode [25,26,28]. The above results entail us that from one aspect, the single-phase semiconductor electrolyte is a suitable candidate for LT-SOFC technology. In contrast, from other aspects, modern thin-film technology is the demand for advanced research technology [37].

Electrochemical impedance spectroscopy

The electrical properties of $SrFe_xTi_{1-x}O_{3-\delta}$($x = 0.2, 0.3$) semiconductor electrolyte were investigated by electrochemical impedance spectroscopy (EIS) under different temperatures

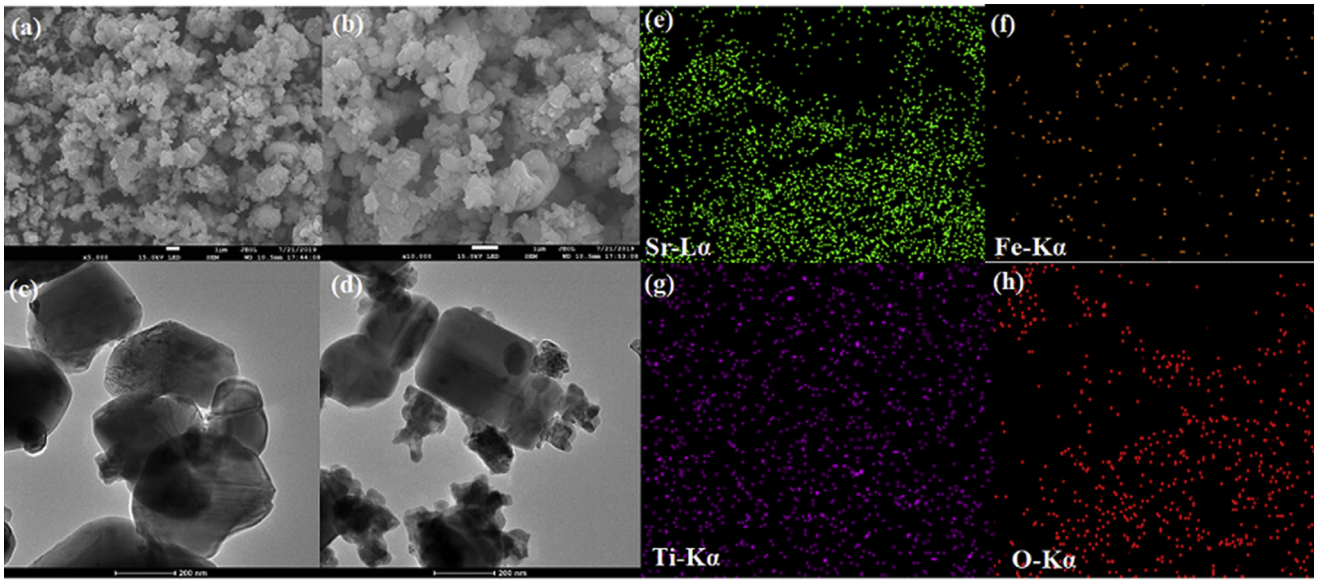

Fig. 2 – (a-b) Scanning electron microscopy (SEM) images of SFT; (c-d) images of HR-TEM of $SrFe_{0.2}TiO_{3-\delta}$ (SFT 20%) and $SrFe_{0.3}TiO_{3-\delta}$ (SFT 30%) at nano-scale level and (e-h) EDX images of $SrFe_xTi_{1-x}O_{3-\delta}$($x = 0.3$).

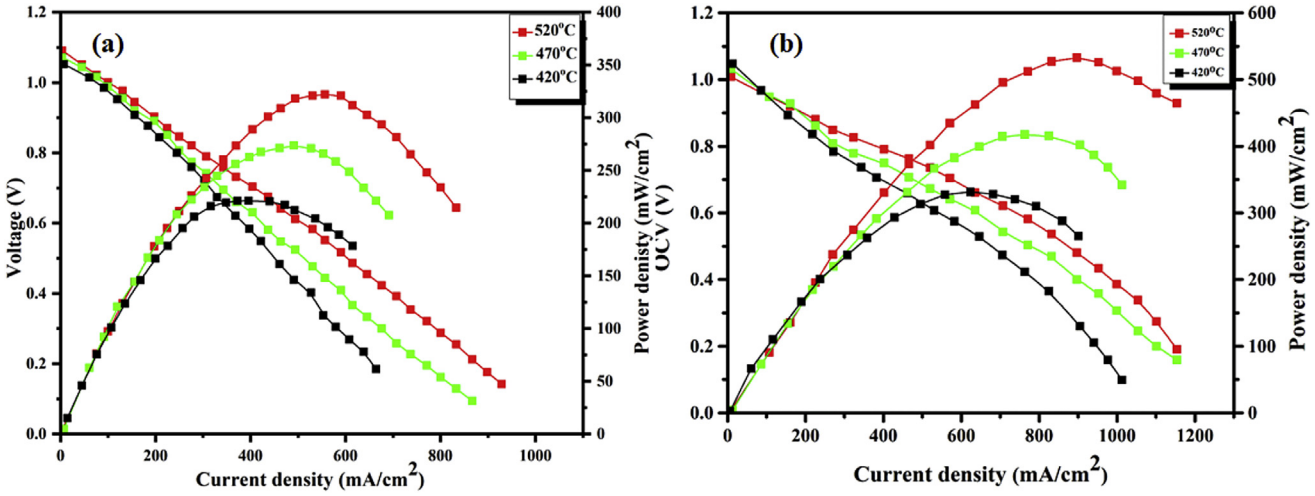

Fig. 3 – (a-b) The fuel cell performance measurements of $SrFe_{0.2}TiO_{3-\delta}$ and $SrFe_{0.3}TiO_{3-\delta}$ as an electrolyte operated at different temperature 420–520 °C.

shown in Fig. 4(a–b). The single-phase semiconductors have specific mechanisms to be incorporated in the fuel cell as an electrolyte; it must possess high ionic conduction and negligible electronic conduction from the traditional aspect. Electrochemical impedance spectroscopy (EIS) was carried out under the H_2/air environment and open-circuit voltage (OCV) conditions at different temperatures 520-420 °C. The entire EIS curve on the real axis, involves the predominant part at high frequency (HF) region, the intersected portion of the curve resides at intermediate frequency range while diminishing semicircle infer into the low-frequency region relates to ohmic resistance, charge, and mass transfer process respectively as explained reported literature [38,39]. The extracted data of EIS is well fitted by employing an equivalent circuit L-R_o(R_1-Q_1) (R_2–Q_2) using zsimpwin software. The fitted circuit includes L represents inductance, R_o is the ohmic resistance due to an electrolyte, R_1 +R_2 = R_p depicts the polarization resistance while Q is the constant phase element (CPE). The extracted data from ZSIMPWIN are presented in Tables 1 and 2.

It can be seen that ohmic resistance R_o for $SrFe_xTi_{1-x}O_{3-\delta}$(x = 0.3) (SFT 30%) electrolyte is 0.06, 0.128 and 0.22 Ω-cm^{-2} and polarization resistance (R_p) is 0.32–1.59 Ω-cm^{-2} at 520, 470 and 420 °C respectively (see Table 2). On the other side, the ohmic resistance (R_o) of $SrFe_xTi_{1-x}O_{3-\delta}$(x = 0.2) (SFT 20%) is 0.45, 0.53 and 0.66 Ω-cm^{-2} and polarization resistance (R_p) value is between 0.53 and 2.09 Ω-cm^{-2} respectively (see Table 1). These results manifest that 30% doping of Fe in $SrTiO_{3-\delta}$ has lower ohmic resistance than 20% Fe doping, as a result, enhanced the ionic conduction of $SrFe_{0.3}TiO_{3-\delta}$ (SFT 30%). Besides, electrode polarization has shown decreasing behavior with an increment of doping proposing the high catalytic activity of electrode. This enhanced activity must be owed to the functionality of electrolyte SFT, which contributes to the electrolyte/electrode part that leads to promote the ORR

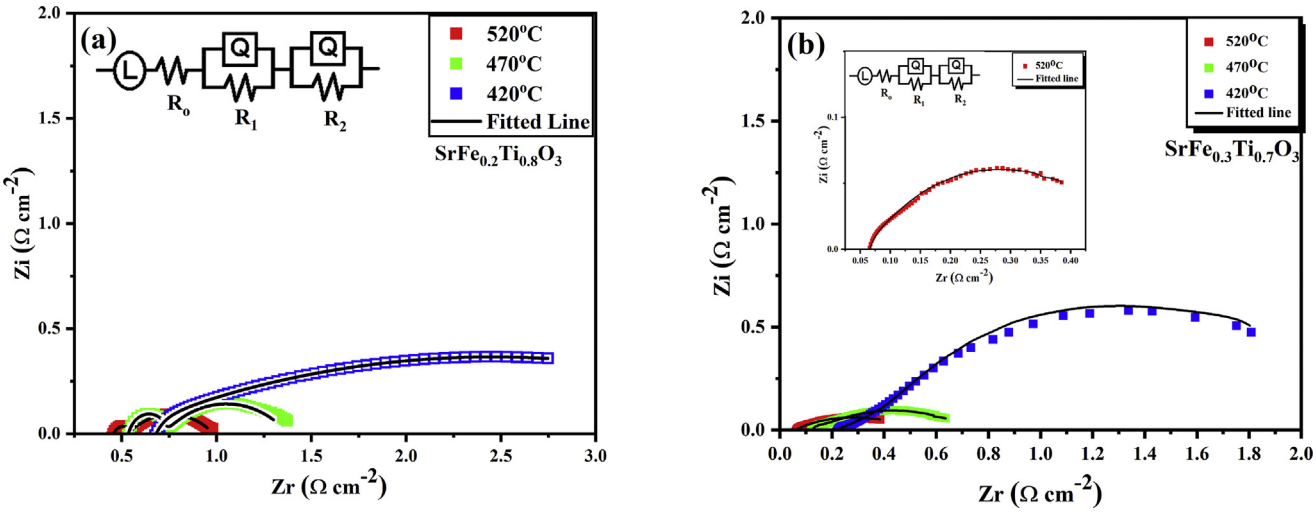

Fig. 4 – (a-b). Electrochemical Impedance (EIS) spectra of $SrFe_xTi_{1-x}O_{3-\delta}$(x = 0.2) and $SrFe_xTi_{1-x}O_{3-\delta}$(x = 0.3) with NCAL electrode operated at different temperature (420–520 °C).

Table 1 – Illustrates the EIS fitted data of $SrFe_xTi_{1-x}O_{3-\delta}$(x = 0.2) (SFT 20%) electrolyte obtained from ZSIMWIN software at different temperatures 420–520 °C.

Composition $SrFe_{0.2}TiO_{3-\delta}$	Inductance (L)	R_o Ω-cm^{-2}	R_1 Ω-cm^{-2}	Q_1 (CPE)	N	C_1	R_2 Ω-cm^{-2}	Q_1 (CPE)	N	C_2
520 °C	1.569E-7	0.45	0.06	7.369E-5	1	7.369E-5	0.47	0.5486	0.4931	0.136187
470 °C	1.779E-7	0.53	0.121	0.3355	0.5245	0.018373	0.749	5.207E-5	0.991	4.74839E-05
420 °C	2.13E-7	0.66	0.812	0.2093	0.2307	5.68E-4	1.278	8.08E-8	0.7177	1.44E-10

Table 2 – Illustrates the EIS fitted data of $SrFe_xTi_{1-x}O_{3-\delta}$(x = 0.3) (SFT 30%) electrolyte obtained from.

Composition $SrFe_{0.3}TiO_{3-\delta}$	Inductance (L)	R_o Ω-cm^{-2}	R_1 Ω-cm^{-2}	Q_1 (CPE)	N	C_1	R_2 Ω-cm^{-2}	Q_2 (CPE)	N	C_2
520 °C	8.214E-8	0.06	0.01	4.03E-7	0.9922	3.460E-7	0.31	1.083	0.3234	0.11039
470 °C	4.116E-8	0.128	0.09	0.01053	0.7222	7.23E-4	0.412	0.4883	0.4001	0.044106
420 °C	7.117E-8	0.22	0.697	0.01251	0.8	3.82E-3	0.893	0.4534	0.7862	0.354568

ZSIMWIN software at different temperatures 420–520 °C.

activity at electrolyte/electrode (SFT/NCAL) interface [25]. Also, NCAL electrodes have a better function, either HOR or ORR, and due to remarkable high conductivity support, the electrochemical reaction can deliver better performance as reported [40–42]. Also, the capacitance value acquired using the following equation$C_i = \frac{(R_i \times Q_i)^{\frac{1}{n}}}{R_i}$. The obtain C_i for (R_1Q_1) and (R_2Q_2) can be related to grain boundary and electrode polarization process as reported elsewhere [22].

Moreover, the ionic conductivity σ_i for $SrFe_xTi_{1-x}O_{3-\delta}$ (x = 0.3) SFT30% and $SrFe_xTi_{1-x}O_{3-\delta}$ (x = 0.2) SFT20% can be calculated from the polarization curve of the polarization region of the I–V curve of fuel cell performance. The central portion in the I–V curve represents the majority of the ohmic portion, which can deliver the ohmic resistance of the electrolyte [43]. The ionic conductivity can be obtained using the following formula σ_i = L/RA where L denotes the pellet thickness, R is the ohmic resistance obtained from the polarization slope while A is an active area of the pellet. The ionic conductivity of $SrFe_xTi_{1-x}O_{3-\delta}$ (x = 0.3) SFT 30% and $SrFe_xTi_{1-x}O_{3-\delta}$ (x = 0.2) SFT 20 %are 0.065–0.17 S/cm and 0.04–0.13 S/cm at 420–520 °C respectively. Such high ionic conductivity is due to the incorporation of Fe, thermal, and an intrinsic property of p-type semiconductor electrolyte. The attained high ionic conductivity of 0.17 S/cm is superior to the reported literature [44–49]. Such high ionic conduction is especially due to the doping of Fe into $SrTiO_3$, which causes to produce more oxygen vacancies that overall enhance the ionic conditions following the charge compensation mechanism. Such as doping of Y into ZrO_2, Fe into YSZ, and doped ceria have reported the high ionic conduction, which could support the ionic transport in SFT electrolyte [50]. Consequently, the activation energy for ionic conduction extracted using the following equation

$$\sigma = \frac{A}{T}\exp\left(-\frac{E_a}{kT}\right)$$

where T represents the temperature, A is an exponential factor, K is Boltzmann constant while E_a represents the activation energy. The activation energy of $SrFe_xTi_{1-x}O_{3-\delta}$ (x = 0.3) SFT 30% for ionic charge carriers is 0.65 eV, which is much lower; therefore, it enables to enhance the performance and ionic conductivity.

UV–visible and UPS analysis

To certify the above results, to understand and propagate the energy band investigation of lessening the electronic flow and enhance the ionic conduction at the interface of electrolyte/electrode. Therefore, the UV and UPS were employed to obtain the results of $SrFe_xTi_{1-x}O_{3-\delta}$ (x = 0.3) SFT 30% and NCAL independently of each component, as depicted in Fig. 5(a–d). The UV–visible absorbance was used to determine the bandgap of the pure semiconductor, either n-type or p-type semiconductor shown in Fig. 5(a–b). The bandgap value can be elucidated using the following relation [51].

$$\alpha h\upsilon = A\left(h\upsilon - E_g\right)^n$$

Following previous reports, the reported bandgap for STO and SFT in SFT-ZnO heterostructure was 3.25 and 2.61 eV, respectively [28,52]. In the current case, $SrFe_xTi_{1-x}O_{3-\delta}$ (x = 0.3) SFT 30% bandgap reduced to 2.54 eV due to the further doping of the dopant; as a result, the conduction of charges enhances because there are more chances of valence electron to move to the conduction band by overcoming the bandgap. Also, the obtained bandgap for NCAL was 1.03 eV, which almost matched the reported elsewhere [53]. The UPS gives the value of VB of SFT and NCAL using the following equation ϕ = 21.2 eV ($E_{cutt\text{-}off} - E_{onset}$) are −7.2 and −6.3 eV respectively as displayed in Fig. 6(c–d) [54]. The CB value obtained by using VB and bandgap is −4.66 eV, and −5.27 eV corresponds to SFT electrolyte and NCAL electrodes, respectively.

Energy band structure for fuel cell design

The charge transport properties in the fuel cell can be explained by designing the materials of the different bandgap. In contrast to the water-splitting process commonly in the fuel cell, electrons are created at the H_2 injection side (Anode/

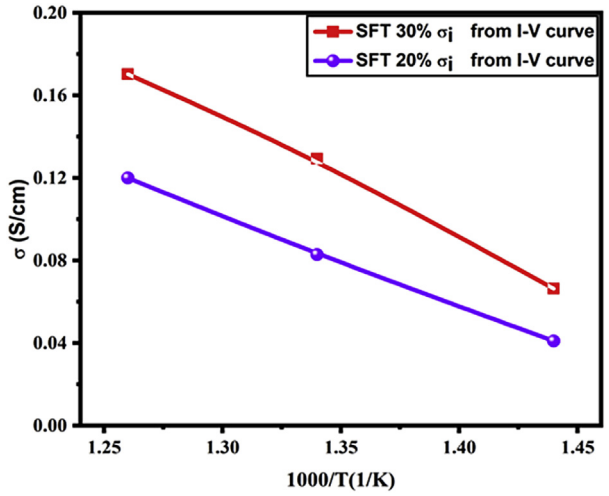

Fig. 5 – Shows the ionic conductivity of $SrFe_xTi_{1-x}O_{3-\delta}$ (x = 0.2) and $SrFe_xTi_{1-x}O_{3-\delta}$ (x = 0.3) as a function of 1000/T at 420–550 °C.

electrolyte) interface, which should follow the external circuit toward cathode to complete the electrochemical reaction especially when the channel is connected. At the same, there should be flow no electron through electrolyte layer; otherwise, short-circuiting occurs, which deteriorates the device. Therefore, it must be diminished by the electrolyte with the help of the energy band theory. There are many examples where electrolytes block electrons from the perspective of energy band theory, such as the CB of YSZ is higher than the redox potential, so the electrolyte prevents electrons [46,55]. Recently dong et al. reported that TiO_2 has a higher conduction level than the anode, so electrons can't jump as a result blocked by an electrolyte [53]. The lower level of the conduction band can cause to be a short-circuiting problem, as observed in SDC [56]. Typically, various four energy band rules should be implied for useful SOFC performance of the device such as $CB_{electrolyte} > H_2/H^+$, $CB_{anode} < H_2/H^+$, $VB_{electrolyte} < O_2/O^{2-}$ and $VB_{anode} > O_2/O^{2-}$ [45].

Following the above rules, we have demonstrated a new larger bandgap electrolyte SFT p-type semiconductor with a higher level of the conduction band at (−4.66 eV). While carefully designed bandgap of a new triple (oxygen ion, electronic, and ionic) conducting electrode NCAL CB (−5.27) was used as a cathode as well as anode [42]. The VB and CB value for SFT and NCAL was elucidated from the UPS is −7.2 eV, −6.3 eV and −4.66 eV, −5.27 eV respectively. Finally, it has concluded from the energy band diagram

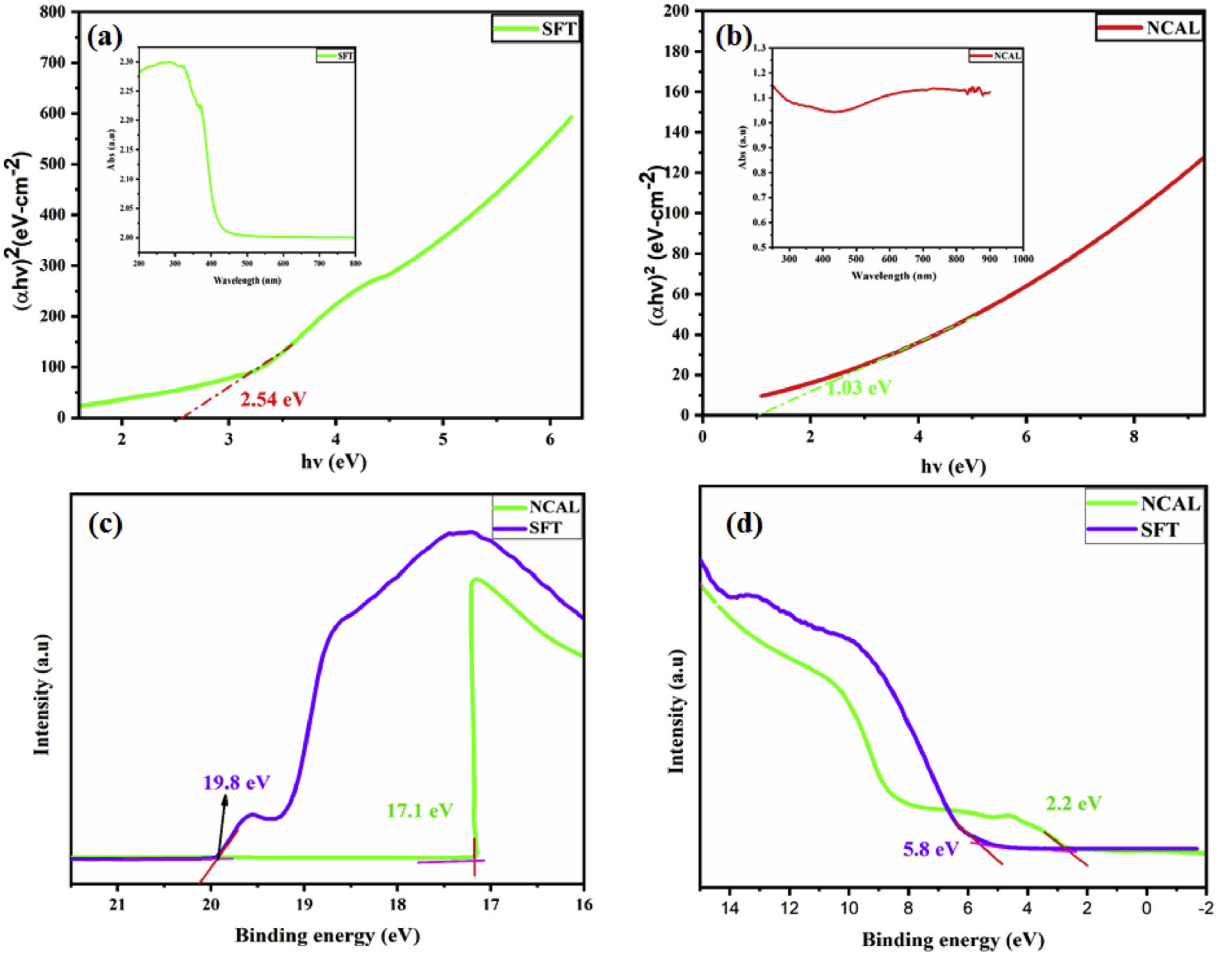

Fig. 6 – (a–b) depicts the UV–visible absorption spectra and bandgap view of the $SrFe_xTi_{1-x}O_{3-\delta}$ (x = 0.3) and NCAL, and (c-d) shows the high and low energy intercept of the UPS for $SrFe_xTi_{1-x}O_{3-\delta}$ (x = 0.3) and NCAL respectively.

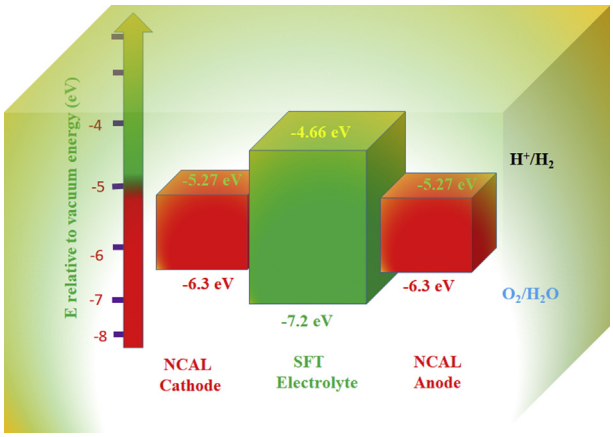

Fig. 7 – Energy band diagram of fuel cell NCAL/SFT/NCAL obtained according to UPS as well as the energy gap of the semiconductor.

that energy levels of these three parts well-matched with above-stated rules, as depicted in Fig. 7. These results guarantee that our device not only gives better performance but also deliver high ionic conduction by diminishing the electronic flow.

Conclusion

In the current study, we synthesized SFT p-type semiconductors via the co-precipitation technique and applied as an electrolyte with symmetrical NCAL electrodes (anode & cathode). The SFT semiconductor electrolyte composition was designed to achieve improved performance of the cell. The cells (Sr_1 $Fe_xTi_{1-x}O_{3-\delta}$ x = 0.2, 0.3), produced a remarkable higher performance of 322 mW/cm^2 and 540 mW/cm^2 along with high ionic conductivity 0.13 S/cm 0.17 S/cm at low-temperature 520 °C respectively. We believe that the improvement in the ionic conduction of SFT electrolyte was primarily due to the generation of O-vacancies created by Fe doping and partly due to the band alignment as a result of Fe doping. Besides, due to doping not only resistance (either ohmic or polarization resistance) reduced but also the bandgap of SFT decreased which strongly favour the higher performance of fuel cell. The high performance of the cells at low temperature successfully demonstrated SFT semiconductor as a potential low temperature electrolyte for SOFC. Moreover, we believe that further engineering in the SFT semiconductor properties can open up new possibilities to utilize this promising material for various other applications of energy technologies.

Acknowledgments

This work was supported by the National Natural Science Foundation of China (NSFC, grant Nos. 11674086, 51774259, 51772080 and 51675496), Engineering Research Center of Nano-Geo Materials of Ministry of Education (NGM2017KF004, NGM2017KF012, and NGM2018KF016). Dr. Asghar thanks the Hubei overseas Talent 100 programme (as distinguished professor at Hubei University) and Academy of Finland (Grant No. 13329016) for their support.

REFERENCES

[1] Zhang W, Wang D, Zheng W. A semiconductor-electrochemistry model for design of high-rate Li ion battery. J Energy Chem 2020;41:100–6. https://doi.org/10.1016/j.jechem.2019.04.018.
[2] Skinner SJ, Kilner JA. Oxygen ion conductors. Mater. Today Off 2003;6:30–7. https://doi.org/10.1016/S1369-7021(03)00332-8.
[3] Wachsman E, Ishihara T, Kilner J. Low-temperature solid-oxide fuel cells. MRS Bull 2014;39:773–9. https://doi.org/10.1557/mrs.2014.192.
[4] Ormerod RM. Solid oxide fuel cells. Chem Soc Rev 2003;32:17–28. https://doi.org/10.1039/B105764M.
[5] Rivera A, Santamaria J, Leon C. Electrical conductivity relaxation in thin-film yttria- stabilized zirconia. Appl Phys Lett 2001;78:610–2. https://doi.org/10.1063/1.1343852.
[6] Wachsman ED, Lee KT. Lowering the temperature of solid oxide fuel cells. Science 2011;334:935–9. https://doi.org/10.1126/science.1204090.
[7] Cao Z, Wang Z, Li F, Maliutina K, Wu Q, He C, Fan L. Insight into high electrochemical activity of reduced La0· 3Sr0· 7Fe0· 7Ti0· 3O3 electrode for high temperature CO2 electrolysis. Electrochim Acta 2020;332:135464. https://doi.org/10.1016/j.electacta.2019.135464.
[8] Meng Y, Wang X, Zhang W, Xia C, Liu Y-n, Yuan M, et al. Novel high ionic conductivity electrolyte membrane based on semiconductor La0. 65Sr0. 3Ce0. 05Cr0. 5Fe0. 5O3-δ for low-temperature solid oxide fuel cells. J Power Sources 2019;421:33–40. https://doi.org/10.1016/j.jpowsour.2019.02.100.
[9] Wang B, Tang L, Qi J, Du H, Zhang ZJ. Synthesis and characteristics of Li- doped ZnO powders for p-type ZnO. J Alloys Compd 2010;503:436–8. https://doi.org/10.1016/j.jallcom.2010.05.028.
[10] Xing Y, Wu Y, Li L, Shi Q, Shi J, Yun S, et al. Proton shuttles in CeO2/CeO2-δ core-shell structure. ACS Energy Lett 2019;11:2601–7. https://doi.org/10.1021/acsenergylett.9b0182.
[11] Zhu B, Fan L, Lund P. Breakthrough fuel cell technology using ceria-based multi-functional nanocomposites. Appl Energy 2013;106:163–75. https://doi.org/10.1016/j.apenergy.2013.01.014.
[12] Fan L, Wang C, Chen M, Zhu B. Recent development of ceria-based (nano) composite materials for low temperature ceramic fuel cells and electrolyte-free fuel cells. J Power Sources 2013;234:154–74. https://doi.org/10.1016/j.jpowsour.2013.01.138.
[13] Wang B, Zhu B, Yun S, Zhang W, Xia C, Afzal M, et al. Fast ionic conduction in semiconductor CeO 2-δ electrolyte fuel cells. NPG Asia Mater 2019;11:1–12. https://doi.org/10.1038/s41427-019-0152-8.
[14] Zhou Y, Guan X, Zhou H, Ramadoss K, Adam S, Liu H, et al. Strongly correlated perovskite fuel cells. Nature 2016;534:231. https://doi.org/10.1038/nature17653.
[15] Zhu B, Raza R, Qin H, Liu Q, Fan L. Fuel cells based on electrolyte and non- electrolyte separators. Energy Environ Sci 2011;4:2986–92. https://doi.org/10.1039/C1EE01202A.
[16] Zhu B, Raza R, Abbas G, Singh M. An electrolyte- free fuel cell constructed from one homogenous layer with mixed

conductivity. Adv Funct Mater 2011;21:2465–9. https://doi.org/10.1002/adfm.201002471.
[17] Fan L, Zhu B, Su P-C, He C. Nanomaterials and technologies for low temperature solid oxide fuel cells: recent advances, challenges and opportunities. Nanomater Energy 2018;45:148–76. https://doi.org/10.1016/j.nanoen.2017.12.044.
[18] Shao K, Li F, Zhang G, Zhang Q, Maliutina K, Fan L, et al. Approaching durable single-layer fuel cells: promotion of electroactivity and charge separation via nanoalloy redox exsolution. ACS Appl Mater Interfaces 2019;11(31):27924–33. https://doi.org/10.1021/acsami.9b08448.
[19] Chen G, Zhu B, Deng H, Luo Y, Sun W, Liu H, et al. Advanced fuel cell based on perovskite La–SrTiO3 semiconductor as the electrolyte with superoxide-ion conduction. ACS Appl Mater Interfaces 2018;10:33179–86. https://doi.org/10.1021/acsami.8b10087.
[20] Chen G, Liu H, He Y, Zhang L, Asghar MI, Geng S, et al. Electrochemical mechanisms of an advanced low-temperature fuel cell with a SrTiO 3 electrolyte. J Mater Chem A 2019;7:9638–45. https://doi.org/10.1039/C9TA00499.
[21] Mi Y, Xia C, Zhu B, Raza R, Afzal M, Riess I. Experimental and physical approaches on a novel semiconducting-ionic membrane fuel cell. Int J Hydrogen Energy 2018;43:12756–64. https://doi.org/10.1016/j.ijhydene.2018.03.204.
[22] Xia C, Mi Y, Wang B, Lin B, Chen G, Zhu B. Shaping triple-conducting semiconductor BaCo 0.4 Fe 0.4 Zr 0.1 Y 0.1 O 3-δ into an electrolyte for low-temperature solid oxide fuel cells. Nat Commun 2019;10:1707. https://doi.org/10.1038/s41467-019-09532-z.
[23] Muhammad Y, Akhtar MN, Shah MAKY, Rauf R, Mushtaq N, Noor A, et al. Evaluation of rare earth (Yb, La) doped (Sm3Fe5O12) garnet ferrite membrane for LT-SOFC. Int J Hydrogen Energy 2020. https://doi.org/10.1016/j.ijhydene.2020.01.166.
[24] Li L, Zhu B, Zhang J, Yan C, Wu Y. Electrical properties of nanocube CeO_2 in advanced solid oxide fuel cells. Int J Hydrogen Energy 2018;43:12909–16.
[25] Mushtaq N, Xia C, Dong W, Abbas G, Raza R, Ali A, et al. Perovskite SrFe1-xTixO3-δ (x<= 0.1) cathode for low temperature solid oxide fuel cell. Ceram Int 2018;44:10266–72. https://doi.org/10.1016/j.ceramint.2018.03.033.
[26] Mushtaq N, Xia C, Dong W, Wang B, Raza R, Ali A, et al. Tuning the energy band structure at interfaces of the SrFe0. 75Ti0. 25O3– δ–Sm0. 25Ce0. 75O2– δ heterostructure for fast ionic transport. ACS Appl Mater Interfaces 2019;42:38737–45. https://doi.org/10.1021/acsami.9b13044.
[27] Baharuddin NA, Muchtar A, Somalu MR. Short review on cobalt-free cathodes for solid oxide fuel cells. Int J Hydrogen Energy 2017;42:9149–55. https://doi.org/10.1016/j.ijhydene.2016.04.097.
[28] Shah MAKY, Mushtaq N, Rauf S, Xia C, Zhu B. The semiconductor SrFe0. 2Ti0. 8O3-δ-ZnO heterostructure electrolyte fuel cells. Int J Hydrogen Energy 2019;44:30319–27. https://doi.org/10.1016/j.ijhydene.2019.09.145.
[29] Yokokawa H, Kawada T, Dokiya M. Thermodynamic regularities in perovskite and K2NiF4 compounds. J Am Ceram Soc 1989;72:152–3. https://doi.org/10.1111/j.1151-2916.1989.tb05971.x.
[30] Yokokawa H, Sakai N, Kawada T, Dokiya M. Thermodynamic stabilities of perovskite oxides for electrodes and other electrochemical materials. Solid State Ionics 1992;52:43–56. https://doi.org/10.1016/0167-2738(92)90090-C.
[31] Chen G, Sun W, Luo Y, He Y, Zhang X, Zhu B, et al. Advanced fuel cell based on new nanocrystalline structure Gd0. 1Ce0. 9O2 electrolyte. ACS Appl Mater Interfaces 2019;11:10642–50. https://doi.org/10.1021/acsami.8b20454.
[32] Pramuanjaroenkij A, Kakaç S, Zhou XY. Mathematical analysis of planar solid oxide fuel cells. In: Mini-micro fuel cells. Springer; 2008. p. 359–90. https://doi.org/10.1007/978-1-4020-8295-5-24.
[33] Duan C, Tong J, Shang M, Nikodemski S, Sanders M, Ricote S, et al. Readily processed protonic ceramic fuel cells with high performance at low temperatures. Science 2015;349:1321–6. https://doi.org/10.1126/science.aab3987.
[34] Saebea D, Authayanun S, Patcharavorachot Y, Chatrattanawet N, Arpornwichanop A. Electrochemical performance assessment of low-temperature solid oxide fuel cell with YSZ-based and SDC-based electrolytes. Int J Hydrogen Energy 2018;43:921–31. https://doi.org/10.1016/j.ijhydene.2017.09.173.
[35] Takagi Y, Lai B-K, Kerman K, Ramanathan S. Low temperature thin film solid oxide fuel cells with nanoporous ruthenium anodes for direct methane operation. Energy Environ Sci 2011;4:3473–8. https://doi.org/10.1039/C1EE01310F.
[36] Tsuchiya M, Lai B-K, Ramanathan S. Scalable nanostructured membranes for solid- oxide fuel cells. Nat Nanotechnol 2011;6:282. https://doi.org/10.1038/nnano.2011.43.
[37] Fan L, Wang C, Osamudiamen O, Raza R, Singh M, Zhu B. Mixed ion and electron conductive composites for single component fuel cells: I. Effects of composition and pellet thickness. J Power Sources 2012;217:164–9. https://doi.org/10.1016/j.jpowsour.2012.05.045.
[38] Zhu B, Raza R, Qin H, Fan L. Single-component and three-component fuel cells. J Power Sources 2011;196:6362–5. https://doi.org/10.1016/j.jpowsour.2011.03.078.
[39] Xia C, Wang B, Cai Y, Zhang W, Afzal M, Zhu B. Electrochemical properties of LaCePr-oxide/K2WO4 composite electrolyte for low-temperature SOFCs. Electrochem Commun 2017;77:44–8. https://doi.org/10.1016/j.elecom.2016.12.013.
[40] Wang B, Cai Y, Xia C, Liu Y, Muhammad A, Wang H, et al. CoFeZrAl-oxide based composite for advanced solid oxide fuel cells. Electrochem Commun 2016;73:15–9. https://doi.org/10.1016/j.elecom.2016.10.005.
[41] Xia C, Wang B, Ma Y, Cai Y, Afzal M, Liu Y, et al. Industrial-grade rare-earth and perovskite oxide for high-performance electrolyte layer-free fuel cell. J Power Sources 2016;307:270–9. https://doi.org/10.1016/j.jpowsour.2015.12.086.
[42] Fan L, Su P-C. Layer-structured LiNi0. 8Co0. 2O2: a new triple (H+/O2–/e–) conducting cathode for low temperature proton conducting solid oxide fuel cells. J Power Sources 2016;306:369–77. https://doi.org/10.1016/j.jpowsour.2015.12.015.
[43] Qiao Z, Xia C, Cai Y, Afzal M, Wang H, Qiao J, et al. Electrochemical and electrical properties of doped CeO2-ZnO composite for low-temperature solid oxide fuel cell applications. J Power Sources 2018;392:33–40. https://doi.org/10.1016/j.jpowsour.2018.04.096.
[44] Garbayo I, Pla D, Morata A, Fonseca L, Sabate N, Tarancon A, et al. Full ceramic micro solid oxide fuel cells: towards more reliable MEMS power generators operating at high temperatures. Energy Environ Sci 2014;7:3617–29. https://doi.org/10.1039/C4EE00748D.
[45] Mahato N, Banerjee A, Gupta A, Omar S, Balani K. Progress in material selection for solid oxide fuel cell technology: a review. Prog Mater Sci 2015;72:141–337. https://doi.org/10.1016/j.pmatsci.2015.01.001.
[46] Prabhakaran K, Beigh M, Lakra J, Gokhale N, Sharma S. Characteristics of 8 mol% yttria stabilized zirconia powder prepared by spray drying process. J Mater Process Technol 2007;189:178–81. https://doi.org/10.1016/j.jmatprotec.2007.01.019.

[47] Fu YP, Wen SB, Lu CH. Preparation and characterization of samaria- doped ceria electrolyte materials for solid oxide fuel cells. J Am Ceram Soc 2008;91:127–31. https://doi.org/10.1111/j.1551-2916.2007.01923.x.
[48] Fabbri E, D'Epifanio A, Di Bartolomeo E, Licoccia S, Traversa E. Tailoring the chemical stability of Ba (Ce0. 8–xZrx) Y0. 2O3– δ protonic conductors for intermediate temperature solid oxide fuel cells (IT-SOFCs). Solid State Ionics 2008;179:558–64. https://doi.org/10.1016/j.ssi.2008.04.002.
[49] Zuo C, Zha S, Liu M, Hatano M, Uchiyama M. Ba (Zr0. 1Ce0. 7Y0. 2) O3–δ as an electrolyte for low-temperature solid-oxide fuel cells. Adv Mat 2006;18:3318–20. https://doi.org/10.1002/adma.200601366.
[50] Gao H, et al. The effect of Fe doping on the properties of SOFC electrolyte YSZ. Solid State Ionics 2008;179(27–32):1620–4. https://doi.org/10.1016/j.ssi.2008.01.040.
[51] Xue F, Huang J, Li T, Wang Z, Zhou X, Wei L, et al. Lowering the synthesis temperature of Y3Fe5O12 by surfactant assisted solid state reaction. J Magn Magn Mater 2018;446:118–24. https://doi.org/10.1016/j.jmmm.2017.08.076.
[52] Wu Y, Dong B, Zhang J, Song H, Yan C. The synthesis of ZnO/SrTiO3 composite for high-efficiency photocatalytic hydrogen and electricity conversion. Int J Hydrogen Energy 2018;43:12627–36. https://doi.org/10.1016/j.ijhydene.2018.03.206.
[53] Dong W, Tong Y, Zhu B, Xiao H, Wei L, Huang C, et al. Semiconductor TiO 2 thin film as an electrolyte for fuel cells. J Mater Chem A 2019;7:16728–34. https://doi.org/10.1039/C9TA01941C.
[54] Li Za, Zhu Z, Chueh C-C, Jo SB, Luo J, Jang S-H, et al. Rational design of dipolar chromophore as an efficient dopant-free hole-transporting material for perovskite solar cells. J Am Chem Soc 2016;138:11833–9. https://doi.org/10.1021/jacs.6b06291.
[55] Liu G, Rodriguez JA, Hrbek J, Dvorak J, Peden CH. Electronic and chemical properties of Ce0. 8Zr0. 2O2 (111) surfaces: photoemission, XANES, density-functional, and NO2 adsorption studies. J Phys Chem B 2001;105:7762–70. https://doi.org/10.1021/jp011224m.
[56] Zhang X, Robertson M, Deċes-Petit C, Qu W, Kesler O, Maric R, et al. Internal shorting and fuel loss of a low temperature solid oxide fuel cell with SDC electrolyte. J Power Sources 2007;164:668–77. https://doi.org/10.1016/j.jpowsour.2006.10.087.